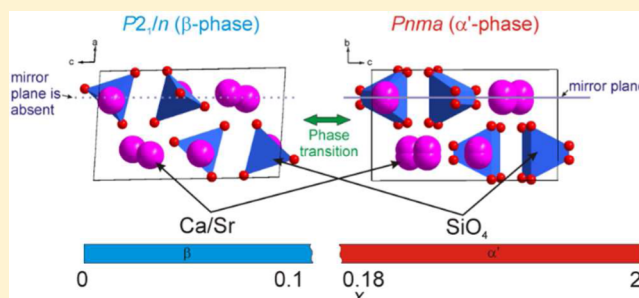


Structural Phase Transformation and Luminescent Properties of $\text{Ca}_{2-x}\text{Sr}_x\text{SiO}_4:\text{Ce}^{3+}$ Orthosilicate PhosphorsMingyue Chen,[†] Zhiguo Xia,^{*,†} Maxim S. Molokeev,^{‡,⊥} and Quanlin Liu[†][†]School of Materials Sciences and Engineering, University of Science and Technology Beijing, Beijing 100083, China[‡]Laboratory of Crystal Physics, Kirensky Institute of Physics, SB RAS, Krasnoyarsk 660036, Russia[⊥]Department of Physics, Far Eastern State Transport University, Khabarovsk 680021 Russia

Supporting Information

ABSTRACT: The orthosilicate phosphors demonstrate great potential in the field of solid-state lighting, and the understanding of the structure–property relationships depending on their versatile polymorphs and chemical compositions is highly desirable. Here we report the structural phase transformation of $\text{Ca}_{2-x}\text{Sr}_x\text{SiO}_4:\text{Ce}^{3+}$ phosphor by Sr^{2+} substituting for Ca^{2+} within $0 \leq x < 2$. The crystal structures of $\text{Ca}_{2-x}\text{Sr}_x\text{SiO}_4:\text{Ce}^{3+}$ are divided into two groups, namely, β phase ($0 \leq x < 0.15$) and α' phase ($0.18 \leq x < 2$), and the phase transition ($\beta \rightarrow \alpha'$) mechanism originated from the controlled chemical compositions is revealed. Our findings verified that the phase transition $Pnma$ (α' -phase) \leftrightarrow $P2_1/n$ (β -phase) can be ascribed to the second-order type, and Sr^{2+} ions in $\text{Ca}_{2-x}\text{Sr}_x\text{SiO}_4$ preferentially occupy the seven-coordinated Ca^{2+} sites rather than the eight-coordinated sites with increasing Sr^{2+} content, which was reflected from the Rietveld refinements and further clarified through the difference of the Ca–O bond length in the two polymorphs of Ca_2SiO_4 . The emission peaks of Ce^{3+} shift from 417 to 433 nm in the composition range of $0 \leq x \leq 0.8$, and the difference in the decay curves can also verify the phase transformation process. Thermal quenching properties of selected $\text{Ca}_{2-x}\text{Sr}_x\text{SiO}_4:\text{Ce}^{3+}$ samples were evaluated, and the results show that the integral emission intensities at 200 °C maintain >90% of that at room temperature suggesting superior properties for the application as white light-emitting diodes (w-LEDs) phosphors.



INTRODUCTION

Recently, orthosilicate phosphors with the general composition of M_2SiO_4 ($\text{M} = \text{Ca}, \text{Sr}, \text{and Ba}$) doped with Eu^{2+} or Ce^{3+} , including the end members or intermediate compositions, have attracted great attention in the field of solid-state white lighting.^{1–5} Understanding of the phase structures of versatile M_2SiO_4 orthosilicate compounds and the structure–property correlation can accelerate the improvement of phosphors for white light-emitting diode (w-LEDs) applications.^{6–9} However, structural phase transformation behaviors in some orthosilicates were not clearly defined until now. Herein, ternary diagram at ambient conditions focusing on any two end members of different phases depending on chemical compositions with general formula $\text{Ca}_{2-x}\text{Sr}_x\text{SiO}_4$, $\text{Ca}_{2-y}\text{Ba}_y\text{SiO}_4$, and $\text{Sr}_{2-z}\text{Ba}_z\text{SiO}_4$ ($0 \leq x, y, z \leq 2$) is first presented in Figure 1a, which is mainly obtained from inorganic structural database (ICSD) and literature. Among them, $\text{Sr}_{2-z}\text{Ba}_z\text{SiO}_4$ compounds show only two phases α'_H and β , and α'_H phase is predominant in a wide composition range.^{1,10,11} This is in accordance with temperature dependences of Ba_2SiO_4 , which shows only α'_H phase under different ambient temperature (Figure 1b), and Sr_2SiO_4 compound, which shows phase transition from β -phase to α'_H -phase under heating. Therefore, small addition of Ba ions in Sr_2SiO_4 compound increases cell volume and has the same

effect as heating of compounds, which induces α'_H -phase. As a comparison, $\text{Ca}_{2-x}\text{Sr}_x\text{SiO}_4$ compounds show diversity of the phases: α'_H -phase; α'_L -phase; β -phase, and γ -phase at ambient conditions.^{2,12–16}

Moreover, it seems to be interesting that α'_H and α'_L phases are not separated into different areas on the ternary diagram but intermixed (Figure 1a). For example, CaSrSiO_4 can exist in α'_H -phase¹⁷ and α'_L -phase¹⁸ at ambient conditions. It seems that these two phases have crystal structures with similar energies, and two allotropic modifications exist. Ca_2SiO_4 also exists in two modifications at ambient conditions: β -phase and γ -phase. Note that α'_L - and α'_H -phases can be induced from Ca_2SiO_4 by heating (Figure 1b).¹⁹ Addition of Sr ion in the Ca_2SiO_4 compound also enlarges cell volume and has the same effect as heating. Therefore, as it was observed in the $\text{Sr}_{2-z}\text{Ba}_z\text{SiO}_4$ crystal system, α'_H -phase can be induced by addition of Sr. However, at some synthesis conditions α'_L -phase also can be induced by addition of Sr, and this diversity of phases can be associated with two modifications β and γ phases of Ca_2SiO_4 compound at ambient conditions.^{20,21} On the basis of the above-mentioned facts on the structural phase

Received: August 28, 2015

Published: November 17, 2015

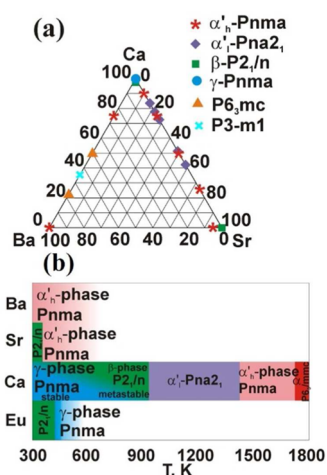


Figure 1. (a) Different phases depending on chemical composition observed in databases and literature of $\text{Ca}_{2-x}\text{Sr}_x\text{SiO}_4$, $\text{Ca}_{2-y}\text{Ba}_y\text{SiO}_4$, and $\text{Sr}_{2-z}\text{Ba}_z\text{SiO}_4$ ($0 \leq x, y, z \leq 2$) compounds on the ternary Ca_2SiO_4 – Sr_2SiO_4 – Ba_2SiO_4 phase diagram at ambient conditions. (b) The reported polymorphs summarization for M_2SiO_4 ($\text{M} = \text{Ba}, \text{Sr}, \text{Ca},$ and Eu) end members depending on temperature.

transformation behaviors in $\text{Ca}_{2-x}\text{Sr}_x\text{SiO}_4$ compounds depending on chemical compositions or temperature, the study of photoluminescence tuning depending on their versatile polymorphs and chemical compositions are highly desirable and discussed in detail in this paper.

Versatile polymorphism of Ca_2SiO_4 has been known for a long time, and the polymorphs of Ca_2SiO_4 established thus far included β , γ , α'_L , α'_{H} , and α phases, as also listed in Figure 1b.^{19,20} Therefore, Ca_2SiO_4 -based phosphor can emit multiple colors depending on different polymorphs and various activator ions. As we know, β - Ca_2SiO_4 can be formed in the normal experimental conditions. However, Ca_2SiO_4 has various phases showing tunable luminescence after doping with Eu^{2+} or Ce^{3+} .^{21,22} For example, $\text{Ca}_2\text{SiO}_4:\text{Eu}^{2+}$ is a green-yellow emitting phosphor, and the emission colors can be apparently shifted from green-yellow to deep red with increasing Eu^{2+} content.³ It is also found that the phase transition $\beta(P2_1/n \text{ space group}) \rightarrow \alpha'_L(Pna2_1 \text{ space group})$ occurred since the amount of dopant Eu^{2+} was controlled between 0.1 and 0.2 mol.¹³ When Al^{3+} ions, which occupied the Si sites, are doped into $\text{Ca}_2\text{SiO}_4:\text{Ce}^{3+}$ the switchover from the blue-emitting β - $\text{Ca}_2\text{SiO}_4:\text{Ce}^{3+}$ to the yellow-emitting γ - $\text{Ca}_2\text{SiO}_4:\text{Ce}^{3+}$ can be achieved.^{2,22}

Inspired by these facts, we assume, in $\text{Ca}_2\text{SiO}_4:\text{Ce}^{3+}$ phosphor, that the substitution by larger Sr^{2+} ion for host cation (Ca^{2+}) can facilitate the phase transition and adjust the luminescent properties, and recently several intermediate compositions in $\text{Ca}_{2-x}\text{Sr}_x\text{SiO}_4$ have been extensively studied, such as CaSrSiO_4 and $\text{Ca}_{1.65}\text{Sr}_{0.35}\text{SiO}_4$. Among them, $\text{CaSrSiO}_4:\text{Eu}^{2+}$ with high Eu^{2+} content has been reported as a red phosphor,²³ and $\text{CaSrSiO}_4:\text{Ce}^{3+}, \text{Li}^+$ phosphor, substituting Al^{3+} for Si^{4+} , has been reported by our group, and the red-shift of the Ce^{3+} emission is ascribed to the polyhedra distortion of the cations.⁵ Eu^{2+} - or Ce^{3+} -doped $\text{Ca}_{1.65}\text{Sr}_{0.35}\text{SiO}_4$ phosphors have become another hot topic recently, and the phase with α'_L crystal structure has been regarded as the high-temperature phase of Ca_2SiO_4 . Tunable luminescence with blue, green, and even red emission can be realized in such a system depending on the different activators and their concentrations.^{24–26} Herein, given the special structural features of $\text{Ca}_2\text{SiO}_4:\text{Ce}^{3+}$,

we select it as a model to study the structural transition through Sr^{2+} cation substitutions. The present research about single Ce^{3+} -doped $\text{Ca}_{2-x}\text{Sr}_x\text{SiO}_4$ phosphors mainly focuses on the development of an appropriate host composition to adjust the switchover from β to α' phase, and the mechanism of the structural transition and the luminescent properties were investigated.

EXPERIMENTAL SECTION

Materials and Preparation. $(\text{Ca}_{1.98-x}\text{Sr}_x\text{Ce}_{0.01}\text{Li}_{0.01})\text{SiO}_4$ phosphors were synthesized by solid-state reaction. CaCO_3 (A.R.), SrCO_3 (A.R.), Li_2CO_3 (A.R.), SiO_2 (A.R.), and CeO_2 (99.99%) starting materials were used as received. Stoichiometric amounts of the required reagents were combined and ground together with a small amount of ethanol using an agate mortar until the mixtures were almost dry (25 min). The charge compensation for the substitution of Ca^{2+} by Ce^{3+} is achieved by adding equimolar concentration of Li^+ . Mixtures were then shifted to the crucible and transferred into the tube furnace to calcine at 1500 °C for 4 h under a reducing atmosphere of N_2 – H_2 (5%). After firing, the samples were cooled to room temperature in the furnace and were ground again.

Characterization. Powder X-ray diffraction (XRD) measurements were performed on a D8 Advance diffractometer (Bruker Corporation, Germany), operating at 40 kV and 35 mA with $\text{Cu K}\alpha$ radiation ($\lambda = 1.5406 \text{ \AA}$). The scanning rate for phase identification was fixed at 8° min^{-1} with a 2θ range from 15° to 60° , and the data for the Rietveld analysis were collected in a step-scanning mode with a step size of 0.02° and 5 s counting time per step over a 2θ range from 5° to 120° . Rietveld refinement was performed by using TOPAS 4.2.²⁷

The room-temperature photoluminescence emission (PL), photoluminescence excitation (PLE) spectral measurements were performed by a fluorescence spectrophotometer (F-4600, HITACHI, Japan) equipped with a photomultiplier tube operating at 400 V, and a 150 W xenon lamp as the excitation source. The luminescence decay curves were obtained using an FLSP9200 fluorescence spectrophotometer (Edinburgh Instruments Ltd., U.K.), and an nF900 flash lamp was used as the excitation resource. The temperature dependence luminescence properties were measured on the same F-4600 spectrophotometer, and it was combined with a self-made heating attachment and a computer-controlled electric furnace (Tianjin Orient KOJI Co., Ltd., TAP-02).

RESULTS AND DISCUSSION

Structural Evolution. The crystal structures of this series of as-prepared $(\text{Ca}_{1.98-x}\text{Sr}_x\text{Ce}_{0.01}\text{Li}_{0.01})\text{SiO}_4$ samples were investigated by using XRD. Considering that the ionic radius of Ce^{3+} is close to that of Ca^{2+} , Ce^{3+} ions substitute for Ca^{2+} sites, and the cosubstitution of $\text{Ce}^{3+}\text{-Li}^+$ for two Ca^{2+} can be used to balance the charge. Since we mainly focus on the phase transformation in the $\text{Ca}_{2-x}\text{Sr}_x\text{SiO}_4$ host by varying the concentration of the Sr^{2+} dopant, the content of the activator ion Ce^{3+} is fixed at 0.01 mol. Figure 2a gives the XRD patterns of $(\text{Ca}_{1.98-x}\text{Sr}_x\text{Ce}_{0.01}\text{Li}_{0.01})\text{SiO}_4$ in the whole range of $0 \leq x < 2$. It is clearly found that the crystal structures of $\text{Ca}_{2-x}\text{Sr}_x\text{SiO}_4$ are divided into two groups, and the phase for the composition at $x = 0.1$ belongs to the β - Ca_2SiO_4 type. However, all the phases are ascribed to the α' - Ca_2SiO_4 type for $x \geq 0.5$, suggesting the formation of a continuous solid solution, which was confirmed by the similar diffraction patterns; the shift of the diffraction peaks to the low 2θ direction originates from the substitution of the bigger ion Sr^{2+} compared to Ca^{2+} . Since we focused on the phase transformation in $(\text{Ca}_{1.98-x}\text{Sr}_x\text{Ce}_{0.01}\text{Li}_{0.01})\text{SiO}_4$, Figure 2b shows the XRD patterns of selected chemical compositions in the range of $0 \leq x \leq 0.8$, and the phase transformation range can be clearly found to be $0.10 \leq x \leq 0.18$ on the basis of the difference in position and relative intensity of the diffraction

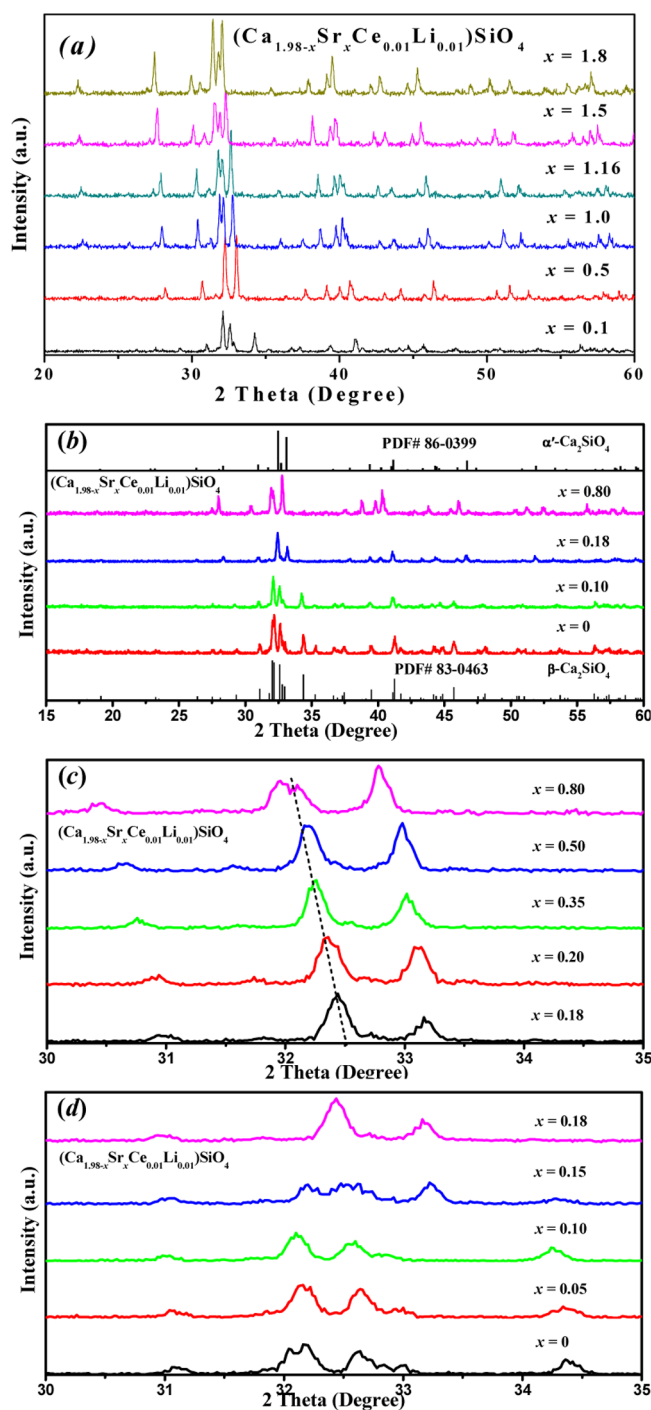


Figure 2. XRD patterns of as-prepared $(\text{Ca}_{1.98-x}\text{Sr}_x\text{Ce}_{0.01}\text{Li}_{0.01})\text{SiO}_4$ samples for different chemical compositions, (a) $x = 0.1, 0.5, 1.0, 1.16, 1.5,$ and 1.8 , (b) $x = 0, 0.18, 0.35,$ and 0.80 . (c) Magnified XRD patterns in the range of $0.18 \leq x \leq 0.8$ for α' - Ca_2SiO_4 . (d) Magnified XRD patterns in the range of $0 \leq x < 0.18$ for β - Ca_2SiO_4 and α' - Ca_2SiO_4 . The standard data of β - Ca_2SiO_4 (PDF card 83–0463) and α' - Ca_2SiO_4 (PDF card 86–0399) are used as reference.

peaks. Moreover, the magnified XRD patterns (shown in Figure 2c,d) recorded over the small range of angles (30° – 35°) for $(\text{Ca}_{1.98-x}\text{Sr}_x\text{Ce}_{0.01}\text{Li}_{0.01})\text{SiO}_4$ clearly illustrate that there are two different phases because of obviously different diffraction peaks in the two phases, namely, β phase ($0 \leq x < 0.15$) and α' phase ($0.18 \leq x < 2$).

To thoroughly understand the detailed changes in the phase transition, powder XRD pattern Rietveld refinements of $(\text{Ca}_{1.98-x}\text{Sr}_x\text{Ce}_{0.01}\text{Li}_{0.01})\text{SiO}_4$ ($x = 0$ to 0.80) were performed. All sites of Ca ions were occupied by Sr ions, and occupancies were refined with assumption that $\text{sum occ}(\text{Ca}) + \text{occ}(\text{Sr}) = 1$ in each site. The results of Rietveld refinement of the powder X-ray patterns of $(\text{Ca}_{1.98-x}\text{Sr}_x\text{Ce}_{0.01}\text{Li}_{0.01})\text{SiO}_4$ samples with different x values are given in Figure 3 for $x = 0.1, 0.15,$ and 0.2

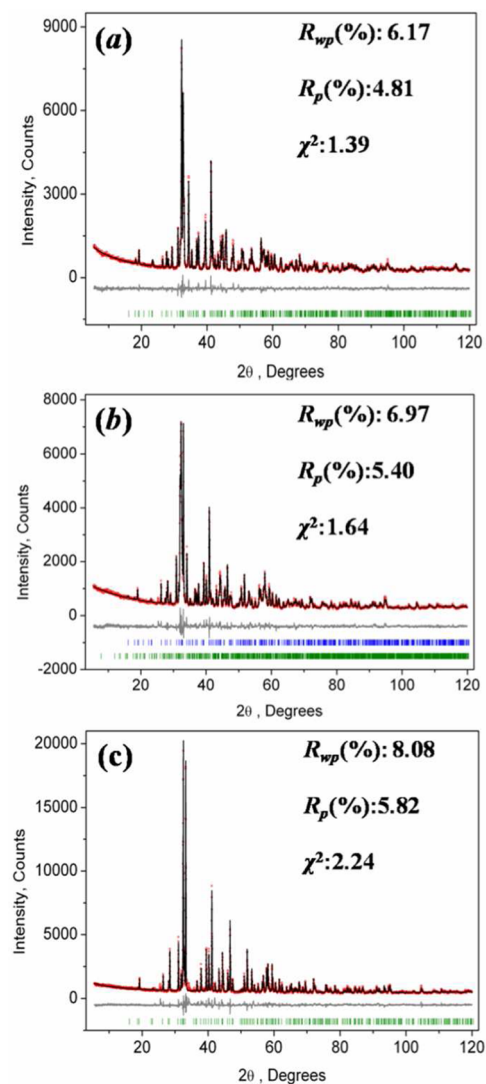


Figure 3. Rietveld refinement of powder XRD profile of the selected compositions of $(\text{Ca}_{1.98-x}\text{Sr}_x\text{Ce}_{0.01}\text{Li}_{0.01})\text{SiO}_4$ with the β -phase, mixed phase and α' -phase, (a) $x = 0.1$, (b) $x = 0.15$, and (c) $x = 0.2$ and the main parameters for the processing and refinement.

and in Figure S1a–f for $x = 0, 0.18, 0.35, 0.50,$ and 0.80 in the Supporting Information, respectively. The main parameters of processing and refinement of the $\text{Ca}_{2-x}\text{Sr}_x\text{SiO}_4$ samples are listed in Table 1. Almost all peaks of $\text{Ca}_{2-x}\text{Sr}_x\text{SiO}_4$ with $x = 0, 0.1$ were indexed by a monoclinic cell ($P2_1/n$) with parameters close to the ones for β - Ca_2SiO_4 reported earlier.²⁸ However, all peaks of $\text{Ca}_{2-x}\text{Sr}_x\text{SiO}_4$ with $x = 0.20, 0.35, 0.50,$ and 0.80 could be easily assigned to the orthorhombic cell ($Pnma$) with parameters close to α' - Ca_2SiO_4 .²⁹ Compounds with $x = 0.15$ and 0.18 showed two-phase system consisting of $P2_1/n$ and $Pnma$ phases. As can be seen from the Rietveld refinement

Table 1. Main Parameters of Processing and Refinement of the $\text{Ca}_{2-x}\text{Sr}_x\text{SiO}_4$ Samples

$\text{Ca}_{2-x}\text{Sr}_x\text{SiO}_4$	space group	phase weight (%)	crystallographic parameters						no. of reflections/parameters
			a (Å)	b (Å)	c (Å)	β (deg)	V (Å ³)	Z	
$x = 0$	$P2_1/n$	100	5.511(7)	6.670(9)	9.317(1)	94.447(8)	346.08(8)	4	516/62
$x = 0.10$	$P2_1/n$	100	5.519(2)	6.781(2)	9.329(3)	94.264(2)	348.26(2)	4	521/66
$x = 0.15$	$P2_1/n$	74(4)	5.521(5)	6.788(7)	9.338(1)	94.126(4)	349.05(6)	4	523/66
	$Pnma$	26(4)	6.787(4)	5.546(4)	9.307(5)	350.33(4)	4	294/62	
$x = 0.18$	$P2_1/n$	9(1)	5.514(2)	6.791(2)	9.334(2)	94.110(2)	348.60(2)	4	523/66
	$Pnma$	91(1)	6.792(2)	5.547(2)	9.309(3)	350.69(2)	4	294/62	
$x = 0.20$	$Pnma$	100	6.791(1)	5.546(9)	9.306(2)		350.49(1)	4	294/62
$x = 0.35$	$Pnma$	100	6.824(1)	5.553(9)	9.326(1)		353.37(9)	4	294/62
$x = 0.50$	$Pnma$	100	6.854(1)	5.560(1)	9.345(1)		356.15(1)	4	296/62
$x = 0.80$	$Pnma$	100	6.912(1)	5.575(8)	9.395(1)		362.01(9)	4	304/62

results for the typical samples of β - Ca_2SiO_4 and α' - Ca_2SiO_4 phases in Figure 3, the refinement was stable and gives low R -factors, and the above results confirm the successive phase transition $\beta \rightarrow \alpha'$ through changing the $\text{Sr}/(\text{Sr} + \text{Ca})$ ratio, so that the concentration of 0.15–0.18 can be considered as critical for the phase transition.

With increasing x in $\text{Ca}_{2-x}\text{Sr}_x\text{SiO}_4$, all the axes (a , b , and c) expand, and the β angle becomes small with eventual increase in the unit-cell volume (V , shown in Figure 4). A good

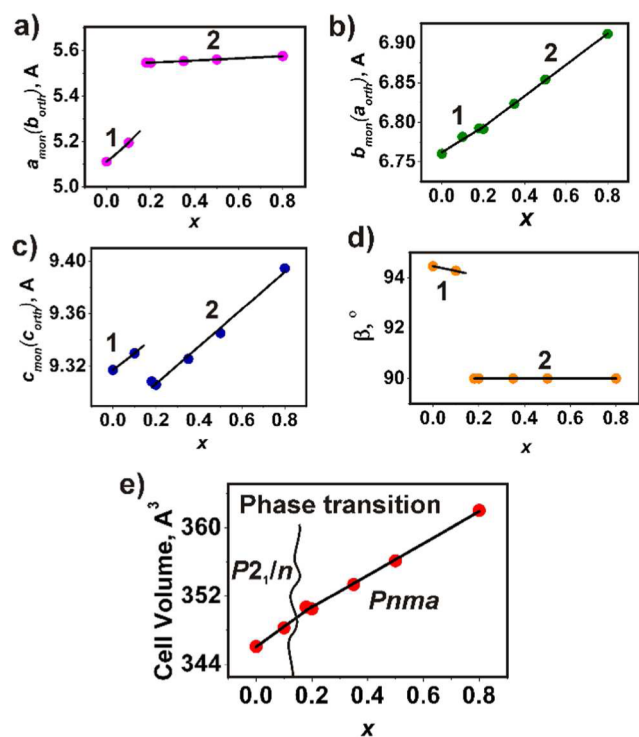


Figure 4. Linear dependence of (a) cell parameters a_{mon} of $P2_1/n$ (1) and b_{orth} of $Pnma$ phase (2); (b) cell parameters b_{mon} of $P2_1/n$ (1) and a_{orth} of $Pnma$ phase (2); (c) cell parameters c_{mon} of $P2_1/n$ (1) and c_{orth} of $Pnma$ phase (2); (d) monoclinic angle β of $P2_1/n$ (1) and $Pnma$ phase (2); (e) cell volume per x in series of compounds $\text{Ca}_{2-x}\text{Sr}_x\text{SiO}_4$.

correlation exists between these cell dimensions and x . The volumetric expansion due to the increment in x from 0 to 0.10 is 0.63% ($\Delta a/a = 0.15\%$, $\Delta b/b = 1.66\%$, $\Delta c/c = 0.13\%$, and $\Delta\beta/\beta = -0.19\%$). These phenomena also exist in the α' - Ca_2SiO_4 phase except for the β angle. The β angle of α' - Ca_2SiO_4 phase is always 90° . The linear dependence of cell volume on x (Figure 4e) also agrees well with Vegard's law and

proves that the suggested chemical formulas are close to real. Cell parameters clearly show that the phase transition ($P2_1/n \leftrightarrow Pnma$) occurs between $x = 0.10$ and $x = 0.20$ (Figure 4a–d).

As is well-known, phase transitions can be divided into first-order and second-order transitions, respectively. The cell volume changes with a discontinuity at the phase transition provided that it belongs to first order. On the contrary, second-order transition has no such jump. In our case, there is no discontinuity in cell volume between $x = 0.1$ and 0.20 (Figure 4e). Therefore, we can conclude that in our case the phase transition $Pnma$ (α' -phase) $\leftrightarrow P2_1/n$ (β -phase) should be of the second-order type. Furthermore, the order–disorder mechanism in α' -phase and the structural transformation $Pnma$ (α' -phase) $\leftrightarrow P2_1/n$ (β -phase) have been investigated in detail.¹⁷ The main interesting results of this investigation are as follows: (1) the $Pnma$ phase can be derived by averaging two $P2_1/n$ asymmetrical configurations related by the (100) mirror plane; (2) all ions besides Si ions in the $Pnma$ phase are disordered between two positions, after the phase transition all ions are ordered (shown in Figure 5); (3) the atomic shifts and rotation

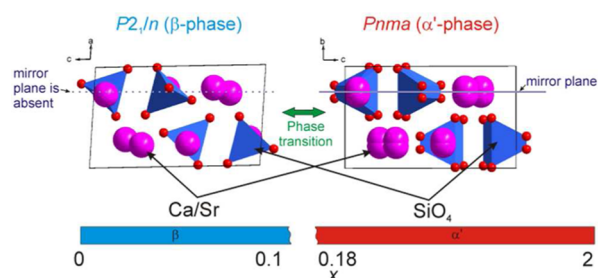


Figure 5. Mechanism of disordering main structural elements in $\text{Ca}_{2-x}\text{Sr}_x\text{SiO}_4$ compounds under phase transition $P2_1/n$ (β -phase) $\leftrightarrow Pnma$ (α' -phase), which occurs between $x = 0.10$ and 0.20 .

angles of the SiO_4 group in $Pnma$ phase increase with increasing x in $\text{Ca}_{2-x}\text{Sr}_x\text{SiO}_4$. Meanwhile, the critical irreducible representation and order parameters that drive this phase transition were also studied. The crystal structure of distorted $P2_1/n$ phase was decomposed into symmetry modes of parent structure $Pnma$ using program ISODISTORT,³⁰ and this revealed two modes: $\Gamma_1^+(e)$ and $\Gamma_3^+(\eta)$ with k vectors $[0, 0, 0]$ and $[0, 0, 0]$, respectively. The e, η are order parameters that are transformed according to the irreducible representations of the space group $Pnma$. ISODISTORT shows that only $\Gamma_3^+(\eta)$ is the critical mode that drives the phase transition, which can be written as $Pnma \rightarrow \{\Gamma_3^+(\eta)\} \rightarrow P2_1/n$. Moreover, based on the group theory, this phase transition is allowed to be second

order, and this is in agreement with smooth cell volume changes with x showed in Figure 4.³⁰

Another thing worthy to be mentioned is that the refined values of Sr concentration in the two sites Ca1/Sr1 and Ca2/Sr2 show almost linear behavior on x (Figure 6). Moreover, the

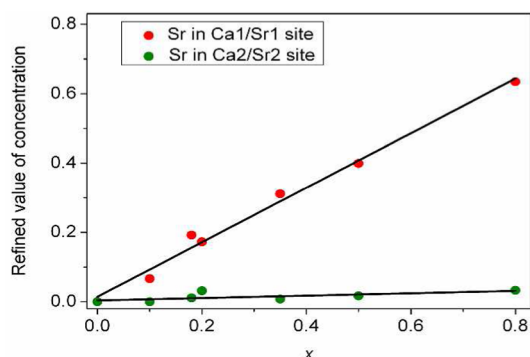


Figure 6. Linear dependence on x of the refined values of the Sr concentration in the two sites Ca1/Sr1 and Ca2/Sr2.

concentration of Sr in Ca2/Sr2 site is almost zero in all samples. Therefore, it can be concluded that small amounts of Sr ($x < 0.15$) in β - Ca_2SiO_4 bring out the results that Sr prefers

to occupy Ca1/Sr1 site. After that, the switchover to orthorhombic phase occurs at the critical value of Sr concentration ($x = 0.15$). The replacement mechanism is not changed by introducing more Sr ($x > 0.15$). The Sr ions still substitute for Ca1/Sr1 site (The specific atomic coordinates and isotropic displacement parameters are shown in Table S1, Supporting Information). This is interesting and unusual, and is ascribed to the fact that the coordination number of Ca1/Sr1 site is seven for β - Ca_2SiO_4 , smaller than the one of Ca2/Sr2 site (that is eight). It is well-known that a bigger coordination number leads to a bigger hole. The reason for this phenomenon is that the Ca–O distances are longer for the smaller hole, as shown in a previous report.¹⁶ Therefore, Sr prefers to occupy a smaller hole rather than a bigger one.

Photoluminescence Evolution. PLE and PL spectra of $(\text{Ca}_{1.98-x}\text{Sr}_x\text{Ce}_{0.01}\text{Li}_{0.01})\text{SiO}_4$ were collected systematically at room temperature. The representative PLE and PL spectra of β phase ($x = 0$) and α' phase ($x = 0.20$) phosphors are shown in Figure 7a,b, respectively. The PLE spectrum of the β phase phosphor consists of three broad bands, which is similar to the previous report.¹⁵ The three-band structure is ascribed to the splitting of a lower triplet and a higher doublet of the $5d$ orbital of the Ce^{3+} ions.²² The emission band is clearly less complex, indicating that, as usual for Ce^{3+} phosphors, only the lowest $5d^1$ state is involved in radiative relaxation. The emission spectrum

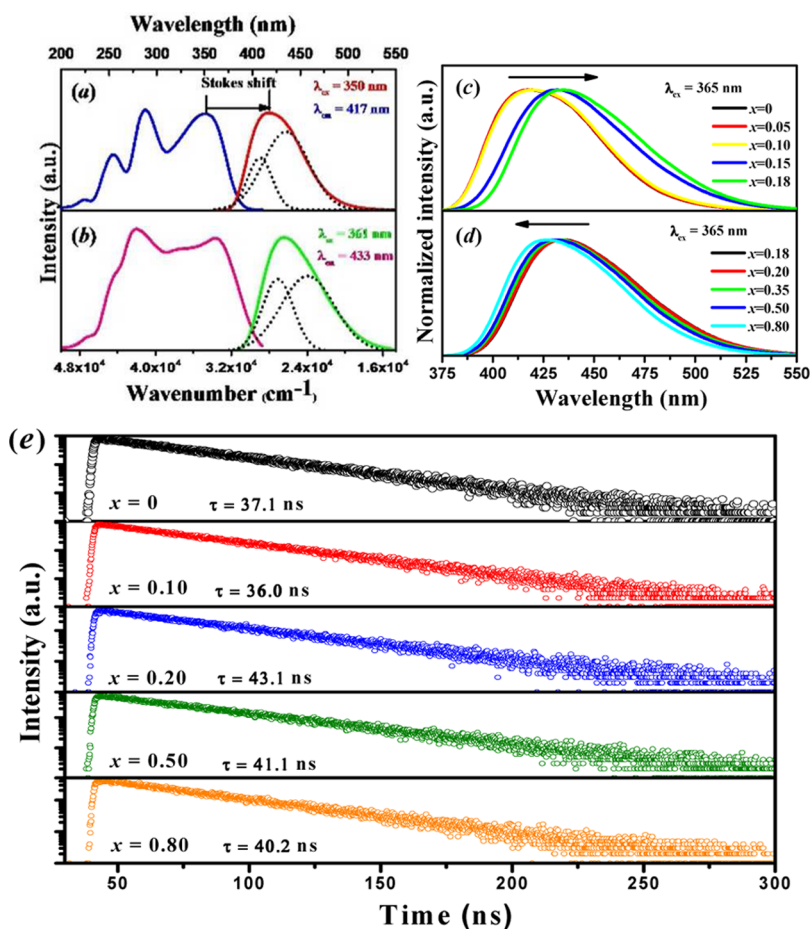


Figure 7. PLE (left) and PL (right) spectra of (a) β phase ($x = 0$) and (b) α' phase ($x = 0.2$) $(\text{Ca}_{1.98-x}\text{Sr}_x\text{Ce}_{0.01}\text{Li}_{0.01})\text{SiO}_4$ phosphors. The approximate spin–orbit splitting of the emission band is represented by two dotted black curves. The normalized emission spectra of (c) β phase phosphors, $(\text{Ca}_{1.98-x}\text{Sr}_x\text{Ce}_{0.01}\text{Li}_{0.01})\text{SiO}_4$ ($x = 0$ to 0.18) and (d) α' phase phosphors ($x = 0.18$ to 0.80) under 365 nm excitation. (e) The decay curves upon 365 nm and lifetime values of Ce^{3+} in $(\text{Ca}_{1.98-x}\text{Sr}_x\text{Ce}_{0.01}\text{Li}_{0.01})\text{SiO}_4$ with different Sr^{2+} content (x), where $x = 0, 0.10, 0.2, 0.5,$ and 0.80 .

shows an obvious broad emission band peaking at 417 nm that can be deconvoluted into two sub-bands peaking at 407 nm ($24\,570\text{ cm}^{-1}$) and 435 nm ($22\,988\text{ cm}^{-1}$), with an energy difference of 1581 cm^{-1} . This energy difference is nearly consistent with the energy difference between the ${}^2F_{7/2}$ and ${}^2F_{5/2}$ states ($1500\text{--}2000\text{ cm}^{-1}$) generated from the 4f level splitting of Ce^{3+} due to spin-orbit coupling, as observed in other Ce^{3+} doped phosphors.³¹ The Stokes shift was estimated to be 4590 cm^{-1} for the β phase $\text{Ca}_2\text{SiO}_4\text{:Ce}^{3+}$ from the PLE/PL spectra in Figure 7a. In light of the XRD results, when the amount of Sr^{2+} substitution is 0.2, α' phase is obtained. Comparing the PLE and PL spectra of β phase with α' phase, some difference in the spectral position and shape can be found. The PLE spectrum of α' phase ($\text{Ca}_{1.98-x}\text{Sr}_x\text{Ce}_{0.01}\text{Li}_{0.01}$)- SiO_4 ($x = 0.2$) phosphor mainly contains two broad bands. The emission band occupies the blue region peaking at 433 nm and shifted to longer wavelength. The energy difference is 1585 cm^{-1} by deconvolution of the emission peak, which is analogous to β phase. The Stokes shift of α' phase is 4605 cm^{-1} , slightly bigger than for the β phase. These values are within the range of those estimated for Ce-doped silicate compounds.³² The comparison of the emission from β and α' phase ($\text{Ca}_{1.98-x}\text{Sr}_x\text{Ce}_{0.01}\text{Li}_{0.01}$)- SiO_4 phosphors can be also observed from the Commission Internationale de l'Eclairage (CIE) chromaticity coordinates. The CIE chromaticity coordinates and the emitting photographs for β - $(\text{Ca}_{1.98}\text{Ce}_{0.01}\text{Li}_{0.01})\text{SiO}_4$ and α' - $(\text{Ca}_{1.78}\text{Sr}_{0.2}\text{Ce}_{0.01}\text{Li}_{0.01})\text{SiO}_4$ phosphors pumped by 365 nm UV lamp are shown in Figure S2. We can see that the CIE coordinate slightly varies from (0.1567, 0.0300) to (0.1493, 0.0568).

The luminescence properties of $(\text{Ca}_{1.98-x}\text{Sr}_x\text{Ce}_{0.01}\text{Li}_{0.01})\text{SiO}_4$ phosphors were comparatively investigated by varying the Sr content between 0 and 0.18 in β phase and 0.18 and 0.80 in α' phase, respectively. The as-measured and normalized emission spectra of $(\text{Ca}_{1.98-x}\text{Sr}_x\text{Ce}_{0.01}\text{Li}_{0.01})\text{SiO}_4$ ($x = 0, 0.05, 0.10, 0.15,$ and 0.18) are illustrated in Figure S3a (see Supporting Information) and Figure 7c; the emission intensities and peak positions keep nearly unchanged for β phase $(\text{Ca}_{1.98-x}\text{Sr}_x\text{Ce}_{0.01}\text{Li}_{0.01})\text{SiO}_4$ ($x \leq 0.1$), and the observed red-shift behaviors should be ascribed to the appearance of α' phase at $x = 0.15$. As discussed above, the intermediate sample with $x = 0.15$ showed a two-phase system consisting of $P2_1/n$ and $Pnma$ phases. When Ce^{3+} ions are doped in β - Ca_2SiO_4 and α' - Ca_2SiO_4 hosts, respectively, the maximum of Ce^{3+} emission spectrum is found to be at 417 and 433 nm, respectively. It is possible to explain the reason why the emission spectra shift to longer wavelength. Although the emission intensities also keep constant for $(\text{Ca}_{1.98-x}\text{Sr}_x\text{Ce}_{0.01}\text{Li}_{0.01})\text{SiO}_4$ ($x = 0.18, 0.20, 0.35,$ and 0.80 ; Figure S3b), an obvious blue shift can be observed from the normalized emission spectra for the α' phase phosphors (Figure 7d), which is ascribed to a crystal field splitting effect.³³ To clarify this fact, the crystal field splitting (Dq) is expressed as follows:

$$Dq = \frac{ze^2r^4}{6R^5}(1) \quad (1)$$

where Dq is the magnitude of the crystal field strength, R is the distance between the central ion and its ligands, z is the charge or valence of the anion, e is the charge of an electron, and r is the radius of the d wave function. In our case, as the average bond length of Sr–O is longer than that of Ca–O in α' - Ca_2SiO_4 , with the doping more Sr ions, the crystal field splitting

becomes smaller, so a blue shift is observed upon replacing the smaller Ca^{2+} ion by the larger Sr^{2+} ion.

Decay behaviors of the activators in the host can act as a useful tool to check the phase transition and site occupancy information.^{34,35} The decay curves upon 365 nm and lifetime values of Ce^{3+} in $(\text{Ca}_{1.98-x}\text{Sr}_x\text{Ce}_{0.01}\text{Li}_{0.01})\text{SiO}_4$ with different Sr²⁺ content (x): $x = 0, 0.10, 0.20, 0.50,$ and 0.80 are demonstrated in Figure 7e. All the decay curves can be well-fitted using a first-order exponential decay formula

$$I(t) = I_0 + A \exp(-t/\tau) \quad (2)$$

where I and I_0 are the luminescence intensity at time t and 0, A is a constant, and τ represents the decay time for an exponential components. The exponential shape of the decay curves is compatible with all Ce^{3+} ions occupying one type of site, which is consistent with the PL spectra observed above. On the basis of the results of single exponential decay fitting, the lifetime values of Ce^{3+} ions in $(\text{Ca}_{1.98-x}\text{Sr}_x\text{Ce}_{0.01}\text{Li}_{0.01})\text{SiO}_4$ phosphors were calculated to be 37.1, 36.0, 43.1, 41.1, and 40.2 ns, for $x = 0, 0.10, 0.20, 0.50,$ and 0.80 , respectively. We also clearly found that there is an obvious difference for the lifetime values for the compositions between $x = 0.10$ and 0.20 suggesting the possible phase transition range. The lifetime of β phase is shorter than for α' phase. Furthermore, there are two distinct types of Ca/Sr sites in the host for the studied $\text{Ca}_{2-x}\text{Sr}_x\text{SiO}_4$ compounds, which implies that two sets of Ce^{3+} centers in $(\text{Ca}_{1.98-x}\text{Sr}_x\text{Ce}_{0.01}\text{Li}_{0.01})\text{SiO}_4$ may be present. To further verify whether two kinds of Ce^{3+} emission centers are existent or not in the typical $(\text{Ca}_{1.98-x}\text{Sr}_x\text{Ce}_{0.01}\text{Li}_{0.01})\text{SiO}_4$ system, the emission decay curves for representative β - $(\text{Ca}_{1.98}\text{Ce}_{0.01}\text{Li}_{0.01})\text{SiO}_4$ and α' - $(\text{Ca}_{1.78}\text{Sr}_{0.2}\text{Ce}_{0.01}\text{Li}_{0.01})\text{SiO}_4$ samples monitored at some selected wavelengths in the corresponding emission spectra are demonstrated in Figure 8a,b, respectively. Depending on different monitoring wavelengths for the two typical samples, the lifetimes of β - $(\text{Ca}_{1.98}\text{Ce}_{0.01}\text{Li}_{0.01})\text{SiO}_4$ increase from 36.0 to 42.1 ns, whereas the lifetime values of α' - $(\text{Ca}_{1.78}\text{Sr}_{0.2}\text{Ce}_{0.01}\text{Li}_{0.01})\text{SiO}_4$ change from 38.7 to 45.3 ns. Therefore, the minor difference in measured fluorescent lifetime also indicates one distribution of similar Ce^{3+} emission center exists in $(\text{Ca}_{1.98-x}\text{Sr}_x\text{Ce}_{0.01}\text{Li}_{0.01})\text{SiO}_4$ phosphor, which is obviously different from a previous report on the presence of two emission centers in α'_L - $(\text{Ca,Sr})_2\text{SiO}_4\text{:Eu}^{2+}$ phosphor.²⁵

Thermal Quenching Properties. Thermal quenching behavior of phosphors is an important factor in evaluating the phosphor for practical application in white LEDs.³⁶ The PL spectra of the representative $(\text{Ca}_{1.98-x}\text{Sr}_x\text{Ce}_{0.01}\text{Li}_{0.01})\text{SiO}_4$ ($x = 0, 0.10, 0.20,$ and 0.80) samples were measured as a function of temperature from 30 to 300 °C. As given in Figure 9, the emission intensities of all samples decrease slightly when the ambient temperature is below 200 °C. It suggests that this series of $(\text{Ca}_{1.98-x}\text{Sr}_x\text{Ce}_{0.01}\text{Li}_{0.01})\text{SiO}_4$ phosphors have excellent thermal stability. As for the selected samples of $(\text{Ca}_{1.98-x}\text{Sr}_x\text{Ce}_{0.01}\text{Li}_{0.01})\text{SiO}_4$, the emission intensities at 200 °C remains 93%, 91%, 93.3%, and 91% of the original intensity at 30 °C for $x = 0, 0.10, 0.20,$ and 0.80 , respectively, shown in Figure 9. The values are very high for the reported orthosilicate phosphors. Additionally, a red shift for the emission peaks with increasing temperature was observed for all the samples, especially for β - $\text{Ca}_{1.9}\text{Sr}_{0.1}\text{SiO}_4\text{:Ce}^{3+}$ ($x = 0.1$). The red-shift behavior is originated from the simultaneous effects of the varied crystal field and the distorted symmetry of the luminescence centers, as also observed in $\text{Sr}_2\text{SiO}_4\text{:Eu}^{2+}$.³⁷ It is believed that the bond length of Ce–O will be increased with

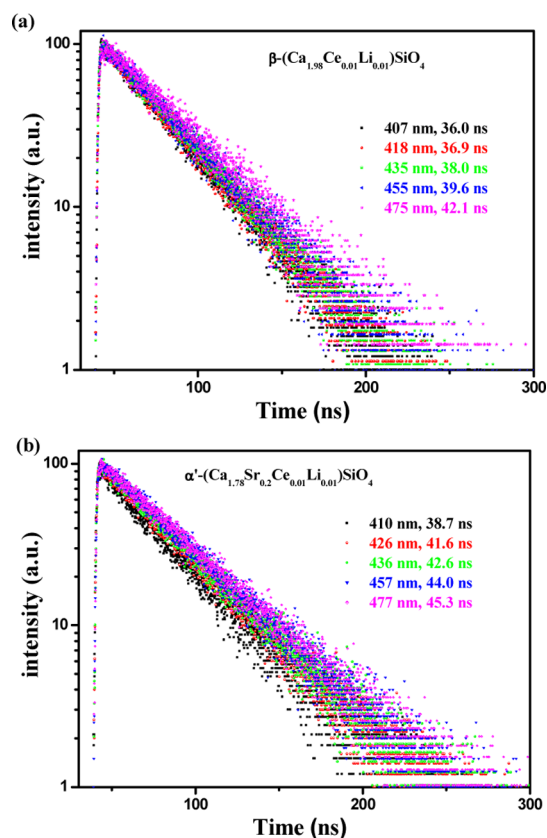


Figure 8. Decay curves and lifetime values for (a) β - $(\text{Ca}_{1.98}\text{Ce}_{0.01}\text{Li}_{0.01})\text{SiO}_4$ and (b) α' - $(\text{Ca}_{1.78}\text{Sr}_{0.2}\text{Ce}_{0.01}\text{Li}_{0.01})\text{SiO}_4$ phosphors monitored at some selected wavelengths in the corresponding emission spectra.

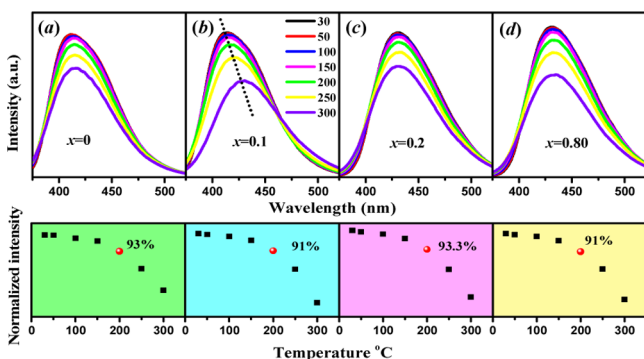


Figure 9. Temperature-dependent emission spectra of $(\text{Ca}_{1.98-x}\text{Sr}_x\text{Ce}_{0.01}\text{Li}_{0.01})\text{SiO}_4$ with Sr^{2+} content (x). β -phase: (a) $x = 0$ and (b) $x = 0.10$; α' phase: (c) $x = 0.20$ and (d) $x = 0.80$ (on the top). Comparison between the luminescence intensities of the $(\text{Ca}_{1.98-x}\text{Sr}_x\text{Ce}_{0.01}\text{Li}_{0.01})\text{SiO}_4$ samples at 200 °C, with respect to the original intensity at 30 °C (at the bottom).

increasing temperature, resulting in the decreased crystal field. However, the symmetry of luminescent center (Ce^{3+}) will be also distorted at high temperature. In such a case as reported in $\text{Sr}_2\text{SiO}_4:\text{Eu}^{2+}$, the induced John–Teller effect is dominant. That is to say, the two effects lead to the splitting of the new excited state or ground state at high temperature.³⁸ Therefore, the transition energy between them will decrease, and the emission peak is observed to be red-shifted with increasing temperature.

Additionally, the internal quantum efficiencies (IQE) of typical samples, β - $(\text{Ca}_{1.98}\text{Ce}_{0.01}\text{Li}_{0.01})\text{SiO}_4$ and α' -

$(\text{Ca}_{1.78}\text{Sr}_{0.2}\text{Ce}_{0.01}\text{Li}_{0.01})\text{SiO}_4$ phosphors, were investigated, and the IQE values were measured upon 365 nm excitation. On the basis of the previous report, the IQE values can be calculated by the following Eq 3.⁴

$$\eta_{\text{IQE}} = \frac{\int L_s}{\int E_R - \int E_S} \quad (3)$$

where L_s represents the luminescence emission spectrum of the sample, E_S is the spectrum of the light used for exciting the sample, and E_R is the spectrum of the excitation light without the sample in the sphere. The corresponding values of β - $(\text{Ca}_{1.98}\text{Ce}_{0.01}\text{Li}_{0.01})\text{SiO}_4$ and α' - $(\text{Ca}_{1.78}\text{Sr}_{0.2}\text{Ce}_{0.01}\text{Li}_{0.01})\text{SiO}_4$ are 63.9% and 51.4%, respectively.

CONCLUSIONS

In summary, the structural phase transformation and the luminescence properties of a series of $\text{Ca}_{2-x}\text{Sr}_x\text{SiO}_4:\text{Ce}^{3+}$ phosphors have been discussed. The crystal structures of $\text{Ca}_{2-x}\text{Sr}_x\text{SiO}_4:\text{Ce}^{3+}$ are divided into two phases, namely, β phase ($0 \leq x < 0.15$) and α' phase ($0.18 \leq x \leq 2$), and the critical concentration of phase transition is $x = 0.15$, as obtained via a combination of optical and structural characterization techniques. The detected phase transition $Pnma$ (α' -phase) \leftrightarrow $P2_1/n$ (β -phase) in $\text{Ca}_{2-x}\text{Sr}_x\text{SiO}_4$ can be ascribed to the second-order type with smooth and linear cell volume variation depending on x , and Sr^{2+} ions in $\text{Ca}_{2-x}\text{Sr}_x\text{SiO}_4$ preferentially occupy the seven-coordinated Ca^{2+} sites rather than the eight-coordinated sites. The emission peaks of Ce^{3+} shift from 417 nm to 433 nm in the range of $0 \leq x \leq 0.8$, and the difference in the decay curves for the two different phases also verified the phase transformation process. Excellent thermal quenching properties of the selected $\text{Ca}_{2-x}\text{Sr}_x\text{SiO}_4:\text{Ce}^{3+}$ samples suggest superior properties for the application as w-LEDs phosphors. This result demonstrated an important understanding on structurally related families of orthosilicate hosts, which also provides an impetus for the exploration of the structure–property relationships of Ce^{3+} - or Eu^{2+} -activated phosphors.

ASSOCIATED CONTENT

Supporting Information

The Supporting Information is available free of charge on the ACS Publications website at DOI: 10.1021/acs.inorgchem.5b01955.

Rietveld refinements, structural data, optical spectra, and CIE chromaticity coordinates diagram for Figures S1–S3 and Table S1. (PDF)

AUTHOR INFORMATION

Corresponding Author

*E-mail: xiazg@ustb.edu.cn.

Notes

The authors declare no competing financial interest.

ACKNOWLEDGMENTS

The present work was supported by the National Natural Science Foundations of China (Grant Nos. 51572023, 51272242, and 5151130035), Natural Science Foundations of Beijing (2132050), the Program for New Century Excellent Talents in Univ. of Ministry of Education of China (NCET-12-0950), Beijing Nova Program (Z131103000413047), Beijing Youth Excellent Talent Program (YETP0635), and the Funds

of the State Key Laboratory of Rare Earth Resource Utilization, Changchun Institute of Applied Chemistry, Chinese Academy of Sciences (RERU2015022).

REFERENCES

- (1) Denault, K. A.; Brgoch, J.; Gaultois, M. W.; Mikhailovsky, A.; Petry, R.; Winkler, H.; DenBaars, S. P.; Seshadri, R. *Chem. Mater.* **2014**, *26*, 2275–2282.
- (2) Kalaji, A.; Mikami, M.; Cheetham, A. K. *Chem. Mater.* **2014**, *26*, 3966–3975.
- (3) Sato, Y.; Kobayashi, M.; Kato, H.; Masaki, T.; Yoon, D.-H.; Kakihana, M. *Angew. Chem., Int. Ed.* **2014**, *53*, 7756–7759.
- (4) Miao, S. H.; Xia, Z. G.; Zhang, J.; Liu, Q. L. *Inorg. Chem.* **2014**, *53*, 10386–10393.
- (5) Miao, S. H.; Xia, Z. G.; Molokeev, M. S.; Chen, M. Y.; Zhang, J.; Liu, Q. L. *J. Mater. Chem. C* **2015**, *3*, 4616–4622.
- (6) Bredig, M. A. *J. Am. Ceram. Soc.* **1950**, *33*, 188–192.
- (7) Liu, J.; Duan, C.-G.; Mei, W. N.; Smith, R. W.; Hardy, J. R. *J. Chem. Phys.* **2002**, *116*, 3864.
- (8) Eysel, W.; Hahn, T. Z. *Kristallogr.* **1970**, *131*, 322–341.
- (9) Park, J. K.; Lim, M. A.; Kim, C. H.; Park, H. D.; Park, J. T.; Choi, S. Y. *Appl. Phys. Lett.* **2003**, *82*, 683–685.
- (10) Barry, T. L. *J. Electrochem. Soc.* **1968**, *115*, 1181–1183.
- (11) Yoo, J. S.; Kim, S. H.; Yoo, W. T.; Hong, G. Y.; Kim, K. P.; Rowland, J.; Holloway, P. H. *J. Electrochem. Soc.* **2005**, *152*, G382–G385.
- (12) Barnes, P.; Fentiman, C. H.; Jeffery, J. W. *Acta Crystallogr., Sect. A: Cryst. Phys., Diffraction, Theor. Gen. Crystallogr.* **1980**, *36*, 353–356.
- (13) Fukuda, K.; Maki, I.; Ito, S.; Ikeda, S. *J. Am. Ceram. Soc.* **1996**, *79*, 2577–2581.
- (14) Yamnova, N. A.; Zubkova, N. V.; Eremin, N. N.; Zadov, A. E.; Gazeev, V. M. *Crystallogr. Rep.* **2011**, *56*, 210–220.
- (15) Hao, Z. D.; Zhang, J. H.; Zhang, X.; Luo, Y. S.; Zhang, L. G.; Zhao, H. F. *J. Lumin.* **2014**, *152*, 40–43.
- (16) Xia, Z. G.; Miao, S. H.; Chen, M. Y.; Molokeev, M. S.; Liu, Q. L. *Inorg. Chem.* **2015**, *54*, 7684–7691.
- (17) Catti, M.; Gazzoni, G.; Ivaldi, G. *Acta Crystallogr., Sect. B: Struct. Sci.* **1984**, *40*, 537–544.
- (18) Il'inets, A. M.; Nevskii, N. N.; Ilyukhin, V. V.; Bikbau, M. Ya.; Belov, N. V. *Dokl. Akad. Nauk SSSR* **1982**, *267*, 641–644.
- (19) Remy, C.; Andrault, D.; Madon, M. *J. Am. Ceram. Soc.* **1997**, *80*, 851–860.
- (20) Nettleship, I.; Slavick, K. G.; Kim, Y. J.; Kriven, W. M. *J. Am. Ceram. Soc.* **1992**, *75*, 2400–2406.
- (21) Itoh, H.; Nishi, F.; Kuribayashi, T.; Kudoh, Y. *J. Mineral. Petrol. Sci.* **2009**, *104*, 234–240.
- (22) Jang, H. S.; Kim, H. Y.; Kim, Y.; Lee, H. M.; Jeon, D. Y. *Opt. Express* **2012**, *20*, 2761–2771.
- (23) Tezuka, S.; Sato, Y.; Komukai, T.; Takatsuka, Y.; Kato, H.; Kakihana, M. *Appl. Phys. Express* **2013**, *6*, 072101–072104.
- (24) Li, K.; Xu, J.; Cai, X. C.; Fan, J.; Zhang, Y.; Shang, M. M.; Lian, H. Z.; Lin, J. *J. Mater. Chem. C* **2015**, *3*, 6341–6349.
- (25) Lu, Z. J.; Mao, Z. Y.; Chen, J. J.; Wang, D. J. *Dalton Trans.* **2015**, *44*, 15620–15627.
- (26) Li, K.; Shang, M. M.; Lian, H. Z.; Lin, J. *Inorg. Chem.* **2015**, *54*, 7992–8002.
- (27) Bruker AXS TOPAS V4: General Profile and Structure Analysis Software for Powder Diffraction Data. *User's Manual*; Bruker AXS: Karlsruhe, Germany, 2008.
- (28) Mori, K.; Kiyonagi, R.; Yonemura, M.; Iwase, K.; Sato, T.; Itoh, K.; Sugiyama, M.; Kamiyama, T.; Fukunaga, T. *J. Solid State Chem.* **2006**, *179*, 3286–3294.
- (29) Mumme, W. G.; Hill, R. J.; Bushnell, G. W.; Segnit, E. R. *Neues Jahrb. Mineral. Abh.* **1995**, *169*, 35–68.
- (30) Campbell, B. J.; Stokes, H. T.; Tanner, D. E.; Hatch, D. M. *J. Appl. Crystallogr.* **2006**, *39*, 607–614.
- (31) Jacobs, R. R.; Krupke, W. F.; Weber, M. J. *Appl. Phys. Lett.* **1978**, *33*, 410–412.
- (32) Liu, Y. W.; Fang, Q.; Ning, L. X.; Huang, Y. C.; Huang, S. Z.; Liang, H. B. *Opt. Mater.* **2015**, *44*, 67–72.
- (33) Duan, C. K.; Reid, M. F. *J. Solid State Chem.* **2003**, *171*, 299–303.
- (34) Chen, X.; Xia, Z. G.; Liu, Q. L. *Dalton Trans.* **2014**, *43*, 13370–13376.
- (35) Shi, M.; Qi, M. M.; Ning, L. X.; Pan, F. J.; Zhou, L.; Zhou, W. J.; Huang, Y. C.; Liang, H. B. *J. Phys. Chem. C* **2015**, *119*, 19326–19332.
- (36) Xia, Z. G.; Liu, R. S.; Huang, K. W.; Drozd, V. J. *Mater. Chem.* **2012**, *22*, 15183–15189.
- (37) Kim, J. S.; Park, Y. H.; Kim, S. M.; Choi, J. C.; Park, H. L. *Solid State Commun.* **2005**, *133*, 445–448.
- (38) Shionoya, S.; Yen, W. M. *Phosphor Handbook*; CRC Press: New York, 1998.